processes

MDPI

Article

Effect of Groundwater Depression Cone on the Hydrochemical Evolution Process in the People's Victory Canal Irrigation Area, China

Shaoyi Feng [1], **Zhongpei Liu** [1,2,*], **Yuping Han** [1,2], **Lu Wang** [1], **Zhipeng Hu** [1] **and Mingkun Qi** [1]

[1] College of Water Resources, North China University of Water Resources and Electric Power, Zhengzhou 450046, China
[2] Henan Key Laboratory of Water Resources Conservation and Intensive Utilization in Yellow River Region, Zhengzhou 450046, China
* Correspondence: liuzhongpei@ncwu.edu.cn

Abstract: The over-exploitation of shallow groundwater in the People's Victory Canal irrigation area has led to the continuous decline in the groundwater level. The formation of a groundwater drawdown cone has changed the original runoff conditions and hydrochemical environment. Based on the groundwater data in the irrigated area from 1996 to 2022, multivariate statistical analysis, traditional hydrochemical methods, and inverse geochemical modeling were used to reveal the impact of the formation of the groundwater depression cone on hydrochemical evolution. The results show that the formation of the groundwater depression cone near the central area in 2003 changed the direction of the canal head flowing to the northwest area, making the groundwater flow from the canal head and the northwest area to the central area. The change in the hydrodynamic fields also caused the groundwater with high salinity in the northwest region to flow to the funnel area, and the ion concentration of groundwater along the pathway area to increase. The groundwater type in the runoff area changes, gradually evolving from Group 1 to Group 2 groundwater. Analysis of the hydrochemical characteristics of groundwater in the runoff area for many years shows that after the formation of the central funnel area in 2003, the groundwater with high SO_4^{2-} ion in the northwest area flows to the funnel area, and the correlation between total dissolved solids and SO_4^{2-} ions in the groundwater along the way is significantly enhanced. The inverse geochemical modeling shows that the main water–rock action along the runoff direction is the dissolution of halite and gypsum. In addition, the study area has a strong cation exchange reaction.

Keywords: groundwater; hydrochemical characteristics; hydrodynamic fields; groundwater depression cone; inverse geochemical modeling

1. Introduction

With the rapid development of the social economy and population growth in recent years, the demand for water resources is also increasing [1]. Intense industrial and agricultural activities make groundwater levels continuously drop, water quality constantly deteriorate, and the amount of groundwater resources available for exploitation and utilization go from bad to worse [2–4]. Due to the lack of management experience and the lack of protection consciousness of groundwater resources, the exploitation and utilization of groundwater, in the long run, is increasing the contradiction between the production. Therefore, it is necessary to systematically study the evolution of the groundwater environment due to the interaction between human activities and natural conditions [5–8].

The evolution process of the groundwater environment is complex, controlled by many fields such as the hydrodynamic field, hydrochemical field, and temperature field, and has high heterogeneity and spatio-temporal variability [9,10]. The characteristics of hydrochemistry are the primary embodiment of the groundwater environment. The

hydrochemical evolution of groundwater is the temporal and spatial variation of various chemical components contained in groundwater. The evolution process is affected by multiple factors, such as hydrogeological conditions, groundwater recharge sources, human activities, and climatic conditions [11–13]. The long-term geochemistry makes the groundwater in different regions form unique hydrochemical characteristics, and the groundwater flow links the groundwater in different regions. Along the flow direction, the water quantity, salinity, and hydrochemical characteristics evolve regularly, presenting a unified spatio-temporal ordered structure [14–16]. The hydrodynamic field is the power source controlling the formation of groundwater flow. The groundwater flow velocity directly determines the time of water-rock and water-water mixing chemical reactions. Generally, the longer the contact time, the more sufficient the response will be and the more complex the hydrochemical characteristics. Before and after the formation of the falling funnel, the dynamic conditions of groundwater will change to a large extent, affecting the reaction direction of the hydrochemical equilibrium. Due to the unique hydrochemical characteristics of different regions, with the flow of groundwater, these characteristic ions can trace the groundwater circulation process, providing a basis for the stable and sustainable development of the groundwater system and environment [17–19].

The People's Victory Canal irrigation area is significant in the middle and lower reaches of the Yellow River. The primary irrigation water plan is Yellow River water, and groundwater is the supplementary water source. Due to the limitation of the height of the diversion gate, the amount of water diverted to the Yellow River decreased, and the groundwater became the primary water supply source in this area [20]. However, the over-exploitation of groundwater leads to the continuous decline of groundwater level, and the scale of the groundwater depression cone is constantly expanding. Moreover, the original natural characteristics of groundwater recharge, runoff, and discharge, and the groundwater hydrochemical environment are changed. At present, the process of groundwater hydrochemical evolution has been well-studied. Many researchers have used multivariate statistical analysis and mineral weathering models to explain the process of aquifer hydrochemical evolution in different hydrogeological systems [21–25]. However, the change in hydrodynamic fields also plays a significant role in groundwater hydrochemical development. There are few studies on the influence of hydrodynamic fields on the evolution of groundwater hydrochemical field [26–29], and the effect of the change of hydrodynamic fields on the development of the hydrochemical process is unclear.

This paper uses multivariate statistical theory to identify differences in groundwater hydrochemical characteristics or the same properties, and draw the change in the groundwater levels in the irrigation area from 1996 to 2022. Combined with the spatial distribution of clusters, the hydrodynamic field changes caused by the groundwater funnel formation were analyzed. Then, the influence of these changes on the hydrochemical evolution of groundwater is discussed. PHREEQC software was used to conduct inverse geochemical modeling of the runoff paths from different areas to the funnel area, to explore the hydrogeochemical reactions occurring on the runoff paths, to identify the influence of the change in hydrodynamic fields on the evolution of hydrochemistry, and to provide a scientific basis for the protection of the groundwater environment in irrigated areas and the formulation of countermeasures for sustainable utilization of groundwater resources.

2. Study Area

The People's Victory Canal irrigation area is located in the north of the Yellow River, Xinxiang City, Henan Province. It is located between Latitude 35°00 N and 35°30 N and Longitude 113°31 E and 114°25 E, and it covers a 1486.84 km^2 area. The climate in the irrigated area is characterized as a warm temperate continental monsoon. The annual mean precipitation is 581.2 mm, and the average evaporation is 1864 mm. Precipitation mainly occurs from July to September, which accounts for more than 70% of the total annual rainfall [30]. Affected by the continuous changes in the Yellow River bank topography, the irrigation area has formed different topographic features, such as depressions, floodplains,

and river channels. These mainly include the low-lying plain of the original extension, the ancient Yellow River beach, the ancient Yellow River back depressions, the Taihang piedmont handover depression, the fortress of Sion, and the Yellow River old road sand dune sand monopoly, Yellow River beach, and Yellow River back river depression (Figure 1). The average annual depth of groundwater in the head of the canal in the irrigation area is about 1–4 m, and that in the northwest area is about 2–7 m. The N02 sampling point in the middle of the irrigation area formed a groundwater depression cone in 2003, and the average depth of groundwater was about 14 m. The average depth of groundwater in the northeast of the irrigation area was about 4–7 m before 2013, and about 9–14 m after 2013. In addition, the dynamic characteristics of groundwater in irrigated areas are also affected by climatic conditions, irrigation water, and artificial exploitation. The groundwater level has prominent seasonal characteristics, mainly as irrigation evaporation.
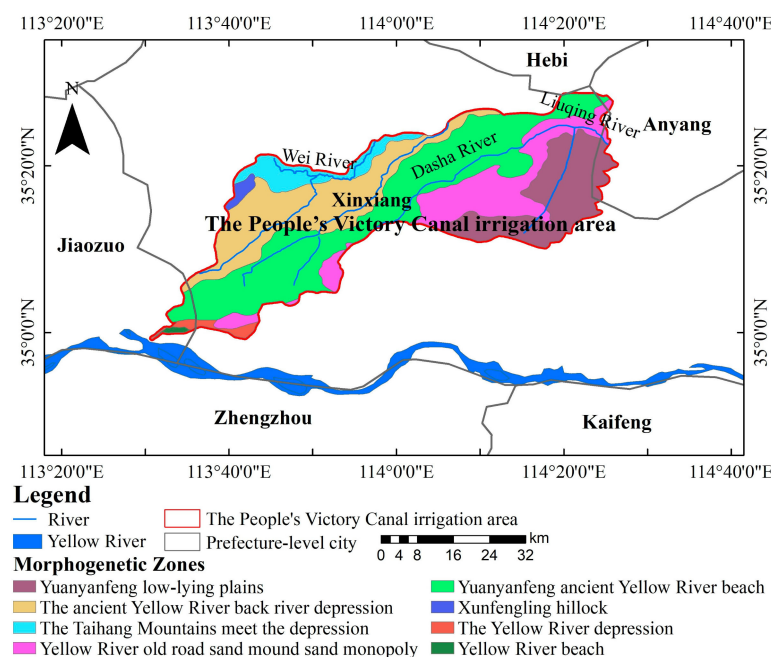

Figure 1. Study area map.

3. Materials and Methods

3.1. Sampling and Measurement

The data used in this paper are the hydrochemistry monitoring data from 1996 to 2013, 2016, and 2022 in the People's Victory Canal irrigation area. The groundwater hydrochemical data from 1996 to 2013 were obtained from the monitoring database of the People's Victory Canal Irrigation Administration of Henan Province. The hydrochemistry data were collected by our research team in 2016 and 2022 using the 425 discrete interval sampler (Solinst, Canada). They were sent to the First Geological and Environmental Survey Institute of Henan Province for testing within 4 days. The main indicators analyzed in this study were: $Na^+ + K^+$, Ca^{2+}, Mg^{2+}, SO_4^{2-}, HCO_3^-, Cl^-, electrical conductivity (EC), and total dissolved solids (TDS). The concentration of Na^+ and K^+ in water samples was determined by flame atomic absorption spectrometry [31]. The concentrations of Ca^{2+} and Mg^{2+} were determined by EDTA titration [32], SO_4^{2-} and Cl^- ion concentrations were measured by ICS−1100 ion chromatography [33], and HCO_3^- ion concentrations were obtained using acid-base titration with an automatic titrator [34]. All samples passed the charge balance test (≤5 %), with the accuracy of each index meeting the quality requirements. All TDS and conductivity data points were measured using portable instruments. The sampling point distribution in the study area is summarized in Figure 2, where the N represents the number of the groundwater sampling point.
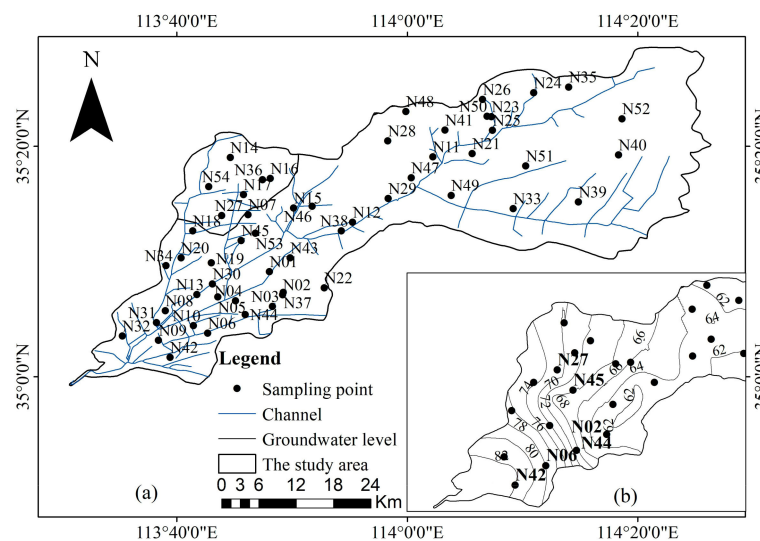
Figure 2. Location map showing sampling site of the study area. ((**a**) is the distribution of all sampling points, (**b**) is sampling points of runoff path selected for inverse geochemical modeling in 2022).

3.2. Data Processing and Analysis

In order to analyze the influence of groundwater flow field changes on groundwater hydrochemical characteristics, it is necessary to draw the groundwater depression cone's generation time and evolution characteristics in the study area. According to the groundwater level data from 1996 to 2022, the Kriging interpolation method of the ArcGIS geostatistics module was used to interpolate the groundwater level spatially, and the annual groundwater level contour map was drawn. The groundwater level contour map showed that the hydrodynamic field changed significantly in 2001, 2003, 2013, and 2022 (Figure 3). Therefore, the groundwater data from 1996, 2001, 2003, 2013, 2016, and 2022 were selected to analyze the influence of flow field change on hydrochemical components.

Multivariate statistical analysis reveals the complex internal relations between hydrochemical samples or indicators by extracting the vital information hidden in the original data group [35–37]. It can more easily summarize the main factors affecting hydrochemical characteristics from many factors and indicators. Systematic cluster analysis is a multivariate statistical method for classifying groundwater based on hydrochemical composition. IBM SPSS Statistics 19 was selected as the data processing software to conduct Q-type cluster analysis on the groundwater data in 1996, 2001, 2003, 2013, 2016, and 2022. In order to avoid the distance between samples being affected by the difference in parameter magnitude, Z-score was used to standardize the groundwater data, and Ward's link method was used to classify the groundwater samples [38,39].

Pearson's correlation (r) has been widely used in the study of hydrochemistry, which allows the determination of relationships between hydrochemical variables [40–42]. When the value of r is more significant than 0.6, it indicates a high correlation, between 0.4 and 0.6, indicating relevance; if the value is less than 0.4, it is irrelevant. The correlation between hydrochemical variables is significant when the test probe is less than 0.05 [43,44]. Due to the regional groundwater in the irrigation area hydrochemical characteristics, we chose specific points on behalf of the regional groundwater hydrochemistry characteristic changes. We selected N17 representative groundwater sampling points for the northwest region. The head of the canal was represented by N05 groundwater sampling points, and by two groundwater runoff area selected sampling points, N01 and N53, respectively. The N02 groundwater sampling point was selected as the representative groundwater point in the funnel area.

In this study, to verify the hydrogeochemical process from the canal head and northwest area to the funnel area, based on the hydrogeological data of the study area and the 2022 groundwater data, the inverse geochemical modeling was used to quantitatively

represent the water–rock interaction process [45–48]. According to the water level of groundwater in 2022 (b), it can be seen that the general runoff direction of groundwater flows from the head of the canal and the northwest region to the central funnel area. Two simulated paths from the head of the canal and the northwest region to the funnel area are determined based on the evolution of hydrochemical types. They are, respectively, N42 → N06 → N44 → N02 and N27 → N45 → N02 (b).
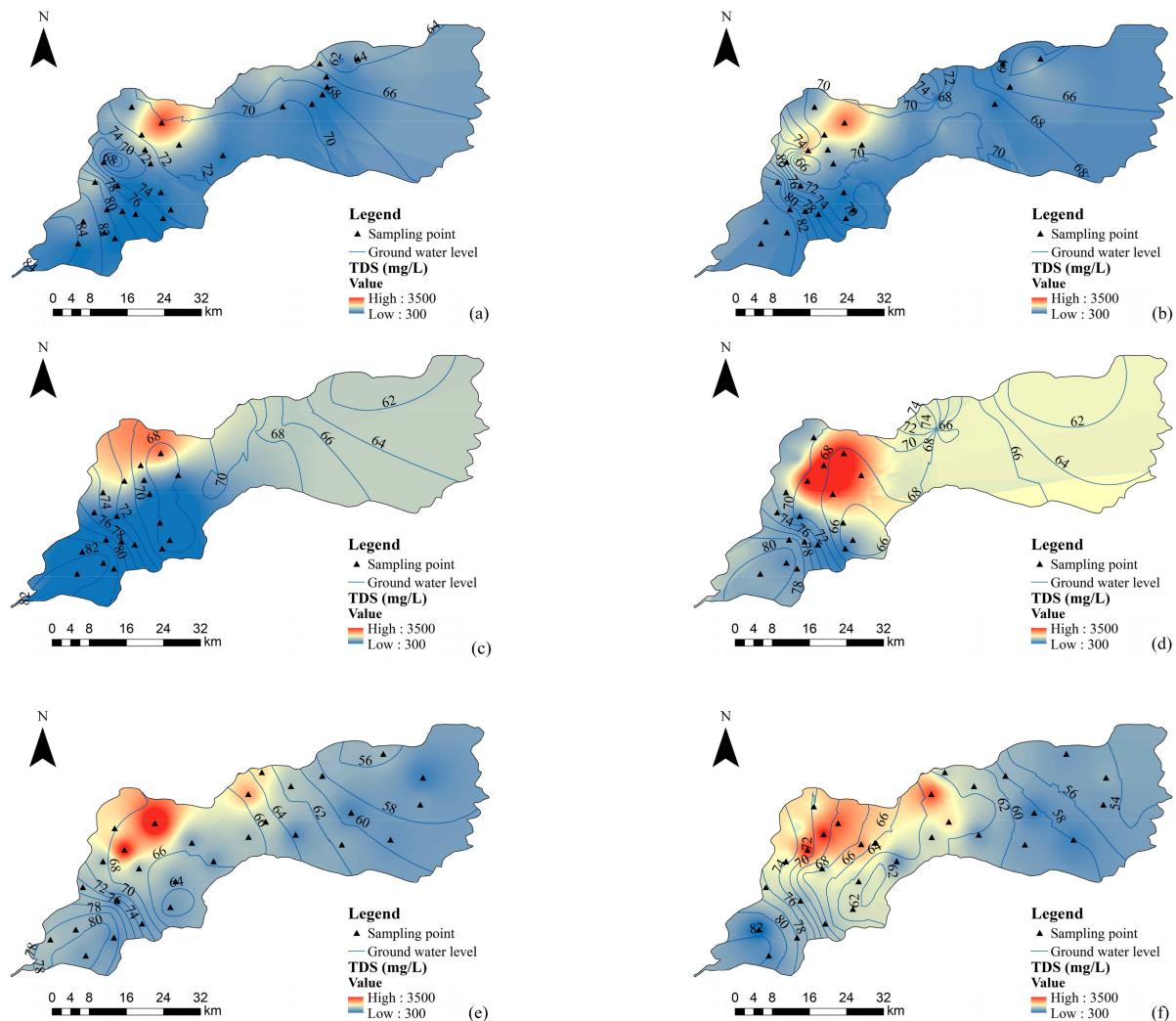

Figure 3. Spatial distribution of groundwater level ((**a**–**f**) are 1996, 2001, 2003, 2013, 2016, and 2022, respectively).

4. Results and Discussion

4.1. Clustering Analysis

Eight indicators of TDS, EC, $Na^+ + K^+$, Ca^{2+}, Mg^{2+}, SO_4^{2-}, HCO_3^-, and Cl^- in groundwater samples were used as variables for cluster analysis. The results of clustering dendrograms based on Ward's method are shown in Figure 4. Cluster analysis divided the groundwater data into three groups, namely, Group 1 (G1), Group 2 (G2), and Group 3 (G3). The main physical and chemical indexes of groundwater in G1, G2, and G3 showed a gradual increasing trend (Figure 5). The cations' concentration in the order of $Na^+ + K^+ > Mg^{2+} > Ca^{2+}$, and the concentration of $Na^+ + K^+$ ions was obviously higher than that of Mg^{2+} and Ca^{2+} ions. It might have something to do with cation exchange. The main anion in G1 and G2 groundwater is HCO_3^-, and the main anion in G3 groundwater is SO_4^{2-}.
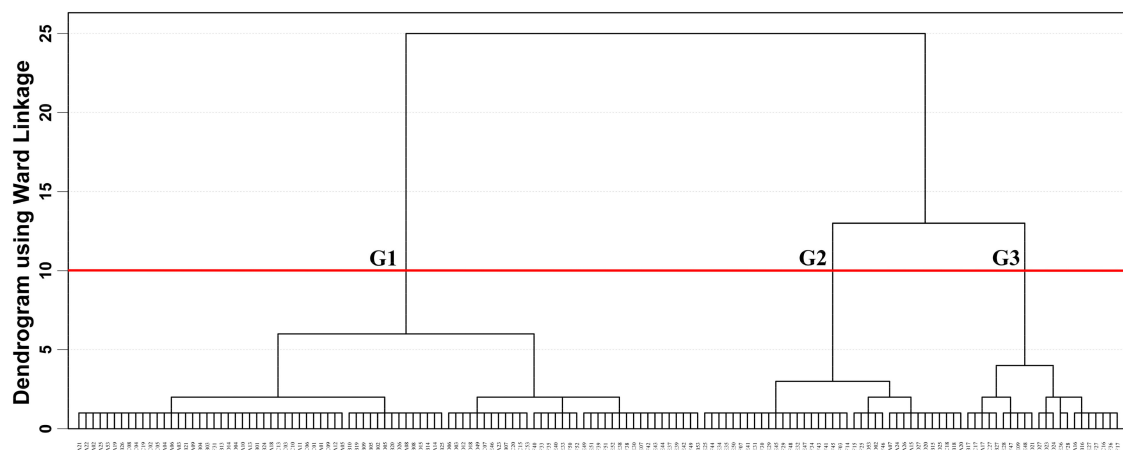
Figure 4. Dendrogram of the Q-mode hierarchical cluster analysis. ((A–F) represent groundwater sampling points in 1996, 2001, 2003, 2013, 2016, and 2022, respectively).
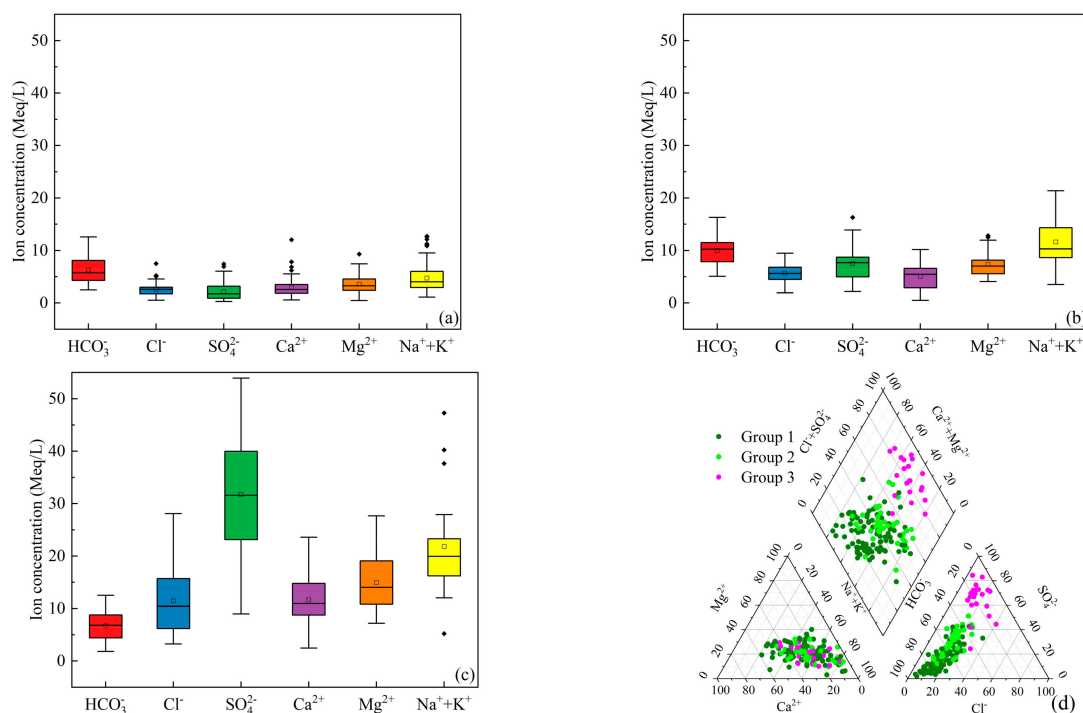

Figure 5. Box diagram of main physical and chemical indicators of cluster group ((**a**–**c**) represent the groundwater ion concentrations of G1, G2, and G3, respectively) and Piper diagram (**d**).

　　　The G1 groundwater included 88 groups of groundwater data, and the TDS concentration ranged from 174.31 mg/L to 1263.80 mg/L, with an average of 582.37 mg/L. The main physicochemical indexes of G1 groundwater were lower than those of G2 and G3 groundwater (Figure 5a–c), and the main hydrochemical types were HCO_3-Na and $HCO_3-Ca \bullet Mg$ (Figure 5d). The G2 groundwater included 37 groups of groundwater data, and the TDS concentration ranged from 804.13 mg/L to 2710.00 mg/L, with an average of 1384.00 mg/L. The main physicochemical indexes of G2 groundwater were significantly higher than those of G1 groundwater, and all the hydrochemical indexes were nearly 50% higher than those of G1 groundwater, especially the SO_4^{2-} ion, which was 71% higher than that of G1 groundwater. The main hydrochemical types are HCO_3-Na and $HCO_3-Ca \bullet Na$. The G3 groundwater includes 22 groups of groundwater data, and the TDS concentration ranges from 2136.20 mg/L to 4431.50 mg/L, with an average of 3148.54 mg/L. Except for HCO_3^- ions, other hydrochemical indexes of G3 groundwater are higher than those of G1 and

G2 groundwater, especially SO_4^{2-} ions, the average concentration of which is as high as 31.78 Meq/L. The main hydrochemical types were $SO_4-Na \bullet Mg \bullet Ca$ and SO_4-Na.

4.2. Groundwater Depression Cone and Clustering Spatial Distribution

The groundwater level in the irrigated area decreased continuously from 1996 to 2022, and the groundwater depression cone and groundwater flow direction also changed. In the irrigated area, except the northwest area, the groundwater level in the field continued to decrease, especially in 2022; the difference between the groundwater level of the funnel area and other areas was the largest. The funnel area of the irrigated area changed from the northwest area to the central area, and the flow direction of groundwater also changed with the formation of the groundwater depression cone. The groundwater level in years with significant changes in the groundwater depression cone is shown in Figure 6. From 1996 to 2001, the funnel's center in the irrigated area was near sampling point N18 in the northwest area (Figure 6a,b). In 2001, the groundwater funnel centered at the sampling point N02 in the middle of the irrigated area began to form gradually. However, at this time, the funnel near the sampling point N18 and the funnel at the sampling point N02 were relatively independent and did not form a unified funnel. In 2003, as the groundwater level continued to drop, the funnel near sampling point N18 connected with sampling point N02, forming a giant groundwater drop funnel (Figure 6c). Figure 6d–f show that the center of the groundwater depression cone gradually shifts to the vicinity of the N02 sampling point with time. The flow direction of groundwater in the head and middle part of the canal also changed with the change of funnel area, from the flow to the northwest area to the flow to the middle area.
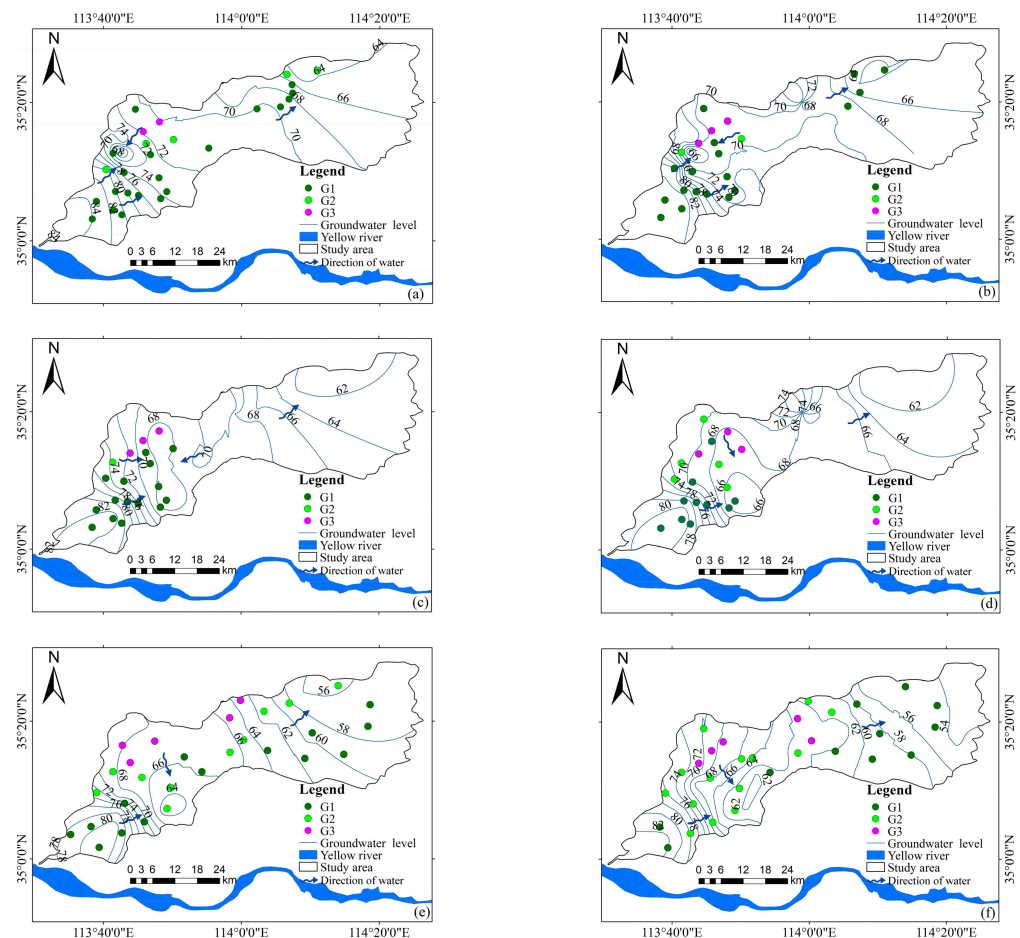

Figure 6. Spatial distribution of clusters representing years ((**a**–**f**) are 1996, 2001, 2003, 2013, 2016, and 2022, respectively).

The results of groundwater clustering analysis in the study area from 1996 to 2022 show spatial and temporal changes. The cluster analysis results in the northwest of the irrigated area have always been dominated by G3 groundwater. The cluster analysis results in the head and middle of the canal have gradually changed from G1 to G2 groundwater. The groundwater in the northwest area has always been dominated by G3 groundwater, which was previously saline-alkali land and had high salinity and high concentration of SO_4^{2-} ion content. From 1996 to 2003, the cluster results of the canal head and central area were mainly G1 groundwater, and the hydrochemical indexes of G1 groundwater were low. G2 groundwater increased in 2013 and 2016 and was mainly distributed between the northwest area and the central funnel area. In 2022, the cluster results of the canal head and the central region were dominated by G2 groundwater. The concentration of ions in G2 groundwater is higher than that in G1 groundwater, especially SO_4^{2-} ion, which increases more than other ions in the same groundwater. SO_4^{2-} ion is the characteristic ion of G3 groundwater, which is the characteristic ion of groundwater in the northwest area, and G2 groundwater is mainly distributed between the northwest area and the central funnel region, indicating that the migration of ions follows the flow of groundwater in the northwest area to funnel region.

In conclusion, the groundwater level in the irrigation area continued to decrease due to the increase in over-exploitation. At the same time, the groundwater depression cone and flow direction also changed, and the hydrochemical field changed with it. In 2003, the formation of a groundwater depression cone near the N02 sampling point in the central region changed the flow direction of the canal head to the northwest region, making the canal head and groundwater in the northwest region flow to the central region. The change in hydrodynamic field causes the change in groundwater type in the runoff area between the northwest area and the funnel area, from G1 to G2 groundwater gradually. The reason for this phenomenon is that the groundwater with the high salinity in northwest area flows to the funnel area, which increases the concentration of groundwater ions in the runoff area along the way.

4.3. Influence of Groundwater Depression Cone on Hydrochemical Evolution

In the process of groundwater flows from the northwest area to the funnel area, the groundwater hydrochemical ions along the way have the hydrochemical characteristics of the northwest area. There is a good correlation between TDS and SO_4^{2-} ion in the groundwater of the northwest area from 1996 to 2013. After the formation of the central funnel area in 2003, the correlation between TDS and SO_4^{2-} ion in the runoff area increased. The groundwater in the northwest area is dominated by G3 groundwater with high salinity and high concentration of SO_4^{2-} ions (Figure 7). The correlation between TDS and SO_4^{2-} ions is high (Figure 7a). The correlation coefficient between TDS and SO_4^{2-} ions at N17 groundwater sampling sites from 1996 to 2013 is as high as 0.92. From 1996 to 2003, the correlation between TDS and SO_4^{2-} ions at groundwater sampling points N01 and N53 in the runoff area was low (Figure 7b,c), and the correlation coefficients were -0.26 and 0.58, respectively. From 2004 to 2013, the correlation between TDS and SO_4^{2-} ions at N01 and N53 groundwater sampling sites increased significantly, with correlation coefficients of 0.98 and 0.89, respectively. The correlation coefficients between TDS and SO_4^{2-} ions at the N02 groundwater sampling site in the funnel area from 1996 to 2003 were 0.82 (Figure 7d). From 2004 to 2013, the correlation coefficients of TDS and SO_4^{2-} ions at the N02 groundwater sampling site were 0.91, respectively, indicating that both the funnel and runoff areas were affected by groundwater flow in the northwest area. There is a good correlation between TDS and HCO_3^- ions (Figure 7e). The correlation coefficient between TDS and HCO_3^- ion at the N05 groundwater sampling site from 1996 to 2013 is as high as 0.85. The correlation coefficients between TDS and HCO_3^- ions at N02 and N53 groundwater sampling points from 1996 to 2013 were 0.87 and 0.52, respectively, indicating that runoff area and funnel area were also affected by groundwater flow at the head of the canal.
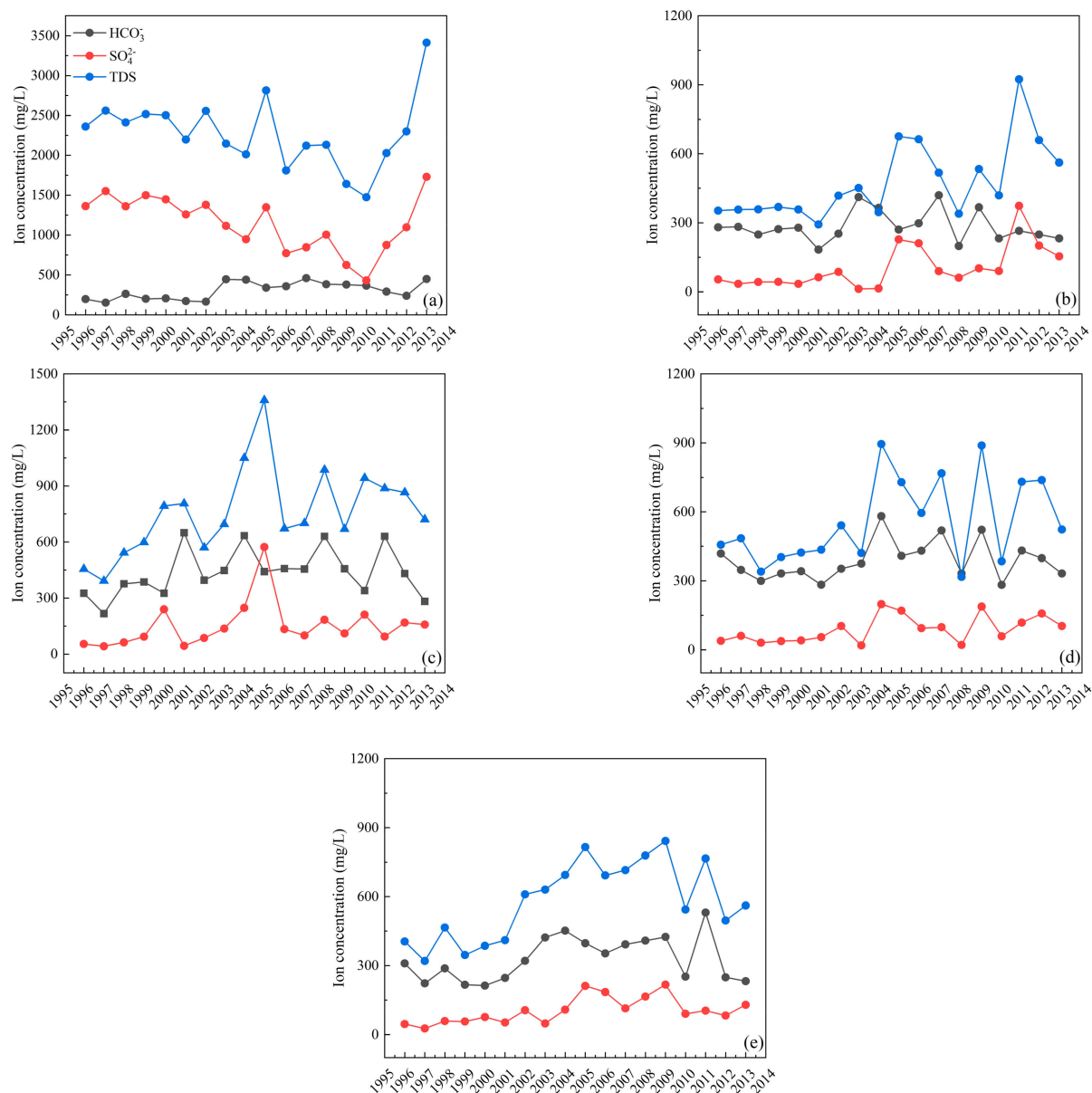
Figure 7. The ion concentration of groundwater sampling points changes over the years ((**a**), N17 sampling sites are located in the northwest region; (**b**), N01 sampling points located in the canal head area; (**c,d**) are N53, N02 sampling points located in the runoff area, and (**e**), N05 sampling point is located in the funnel area).

After the formation of the central funnel area in 2003, the groundwater flowing through the northwest region to the funnel area is affected by the high SO_4^{2-} ions in the northwest region, so the correlation between TDS and SO_4^{2-} ions is significantly enhanced. In addition, the correlation between TDS and HCO_3^- ions in the runoff area and funnel area are increased by groundwater at the head of the canal.

4.4. Inverse Geochemical Modeling

Inverse geochemical modeling uses material balance models to determine the amount of mineral precipitation or dissolution between different points along the groundwater runoff path. It applies to water and rock components to identify and quantify hydrogeochemical reactions, thereby explaining hydrochemical composition evolution. The selection of possible mineral facies is a crucial step for the success of inverse geochemical modeling, which is mainly based on hydrochemical analysis, rock and mineral identification, and

characteristics of the water-bearing medium. According to the previous hydrochemical analysis of the study area, the main mineral phases include calcite, dolomite, halite, gypsum, kaolinite, and k-mica. In the process of hydrochemical evolution, cation exchange is essential and should be taken as a mineral phase. Considering that $CO_2(g)$ will continuously dissolve into groundwater, $CO_2(g)$ is also a possible mineral phase. The simulation results are shown in Table 1.

Table 1. Inverse geochemical modeling of groundwater path simulation results (unit: mmol/L).

Mineral Phase	Chemical Formula	Runoff Path 1			Runoff Path 2	
		N42-N06	N06-N44	N44-N02	N27-N45	N45-N02
Dolomite	$CaMg(CO_3)_2$	1.67				
Calcite	$CaCO_3$	−1.41				
Gypsum	$CaSO_4 \bullet 2H_2O$	1.33	0.75	1.80	0.37	12.67
Halite	NaCl	1.66				2.71
CaX_2	CaX_2	−0.77	−0.12	−0.51		−10.40
NaX	NaX	1.53	0.25	1.02	−3.00	16.13
MgX_2	MgX_2				1.50	2.33
Kaolinite	$Al_2Si_2O_5(OH)_4$		0.06	−0.11	−0.08	−0.88
K-mica	$K(Mg,Fe)_3AlSi_3O_{10}(F,OH)_2$		−0.04	0.08	0.05	0.59
$CO_2(g)$	CO_2		−0.50	0.78	1.35	−1.37

Note: The positive value indicates that the mineral phase dissolves and enters the groundwater; negative values indicate that mineral phases precipitate out of groundwater.

The simulation results are analyzed as follows:

Runoff path 1 (N42 → N06 → N44 → N02): From the N42 to N06 sampling point of the canal head, the dissolution of dolomite, gypsum, and halite occurs, and calcite precipitation occurs. In addition, there is a positive cation exchange effect, which makes the Na^+ ion in the soil enter the groundwater. The hydrogeochemical reactions from N06 to N44 and N44 to N02 were similar, with gypsum dissolution and positive cation exchange. Weak kaolinite dissolution and k-mica precipitation also occurred from N06 to N44, while kaolinite precipitation and k-mica dissolution occurred from N44 to N02.

Runoff path 2 (N27 → N45 → N02): From N27 to N45 sampling point, weak dissolution of gypsum and biotite occurred, and precipitation of kaolinite occurred. Unlike the cation exchange reaction in other paths, reverse cation exchange occurred here, and Na^+ ion was exchanged into the surrounding soil, while Mg^{2+} ion was exchanged into groundwater. There are many hydrogeochemical reactions between the N45 and N02 sampling points; gypsum, halite, and k-mica are dissolved, and only kaolinite is precipitated. In addition, the positive cation exchange along this path is robust, and Na^+ and Mg^{2+} ions in the soil enter into the groundwater, and Ca^{2+} in groundwater enter into the soil.

According to the inverse geochemical modeling results, the main water–rock interactions in the runoff direction are the dissolution of halite and gypsum, dolomite, calcite precipitation, local dissolution and precipitation of kaolinite and quartz, and carbon dioxide spillover. In addition, the study area has a strong cation exchange reaction.

5. Conclusions

The groundwater data can be divided into three groups by clustering analysis. The main physical and chemical indexes of groundwater in the G1, G2, and G3 show a gradually increasing trend. The cations concentration in the order is $Na^+ + K^+ > Mg^{2+} > Ca^{2+}$, and the primary anion in G1 and G2 groundwater is HCO_3^-. The main hydrochemical types are HCO_3-Na, $HCO_3-Ca \bullet Mg$ and $HCO_3-Ca \bullet Na$. The main anions in G3 groundwater are SO_4^{2-}, and the main hydrochemical types are $SO_4-Na \bullet Mg \bullet Ca$ and SO_4-Na.

The groundwater depression cone was located in the northwest area from 1996 to 2003 and gradually moved to the vicinity of the N02 sampling point in the central area after 2003, which changed the hydrodynamic field. The groundwater flows from the canal's head to the northwest area, which was changed to the central funnel area. In addition,

the groundwater in the northwest area also flowed to the central funnel area. This change resulted in the change of groundwater types in the area through which the northwest region flows to the funnel area. The ion concentration of groundwater in the area along the way increased, gradually evolving from G1 to G2 groundwater.

After analyzing the characteristics of groundwater chemical changes in the canal head, runoff area, and funnel area for many years, it was found that, after the formation of the central funnel area in 2003, the groundwater with high SO_4^{2-} ion in the northwest area flows to the funnel area, and the correlation between TDS and SO_4^{2-} ion in the groundwater along the way is significantly enhanced. In addition, the canal head groundwater also increases the correlation between TDS and HCO_3^- ion in the runoff and funnel areas.

The inverse geochemical modeling shows that the main water–rock interactions of groundwater along the runoff direction are the dissolution of halite and gypsum, the dissolution of dolomite, the precipitation of calcite, and the dissolution and precipitation of kaolinite and quartz, and the spillover of carbon dioxide. In addition, the study area has a strong cation exchange reaction.

Author Contributions: S.F.: Writing—original draft, Methodology, Writing—review & editing. Z.L.: Writing—original draft, Writing—review & editing. Y.H.: Supervision, Writing—review & editing. L.W.: Supervision, Writing—review & editing. Z.H.: Supervision, Writing—review & editing. M.Q.: Supervision, Writing—review & editing. All authors have read and agreed to the published version of the manuscript.

Conflicts of Interest: There are no conflict to declare.

References

1. Wu, Y.Z.; Pan, C.F.; Lin, Y.; Cao, F.L.; Wang, Z.J. Hydrogeochemical characteristics and controlling factors of main water filled aquifers in the typical North China coalfield. *Bull. Geol. Sci. Technol.* **2018**, *37*, 191–199. [CrossRef]
2. Asmael, N.M.; Huneau, F.; Garel, E.; Celle-Jeanton, H.; Le Coustumer, P.; Dupuy, A. Hydrochemistry to delineate groundwater flow conditions in the Mogher Al Mer area (Damascus Basin, Southwestern Syria). *Environ. Earth Sci.* **2014**, *72*, 3205–3225. [CrossRef]
3. Chen, J.; Gao, Y.Y.; Qian, H.; Ren, W.H.; Qu, W.G. Hydrogeochemical evidence for fluoride behavior in groundwater and the associated risk to human health for a large irrigation plain in the Yellow River Basin. *Sci. Total Environ.* **2021**, *800*, 149428. [CrossRef] [PubMed]
4. Wang, W.; Chen, Y.N.; Wang, W.H.; Xia, Z.H.; Li, X.Y.; Kayumba, P.M. Hydrochemical characteristics and evolution of groundwater in the dried-up river oasis of the Tarim Basin, Central Asia. *J. Arid. Land* **2021**, *13*, 977–994. [CrossRef]
5. Yuan, H.; Yang, S.; Wang, B. Hydrochemistry characteristics of groundwater with the influence of spatial variability and water flow in Hetao Irrigation District, China. *Environ. Sci. Pollut. Res.* **2022**, *29*, 71150–71164. [CrossRef] [PubMed]
6. Xiao, J.; Lv, G.; Chai, N.; Hu, J.; Jin, Z. Hydrochemistry and source apportionment of boron, sulfate, and nitrate in the Fen River, a typical loess covered area in the eastern Chinese Loess Plateau. *Environ. Res.* **2022**, *206*, 112570. [CrossRef]
7. Wang, L.; He, Z.; Li, J. Assessing the land use type and environment factors affecting groundwater nitrogen in an arid oasis in northwestern China. *Environ. Sci. Pollut. Res.* **2020**, *27*, 40061–40074. [CrossRef]
8. Yang, Q.C.; Li, Z.J.; Xie, C.; Liang, J.; Ma, H.Y. Risk assessment of groundwater hydrochemistry for irrigation suitability in Ordos Basin, China. *Nat. Hazards* **2020**, *101*, 309–325. [CrossRef]
9. Guo, X.J.; Wang, W.H.; Wang, J.S.; Wang, W. Hydrochemical characteristics and evolution pattern of groundwater system in Baiyangdian wetland. North Chian Plain. *Acta Geol. Sin.* **2022**, *96*, 656–672. [CrossRef]
10. Rodriguez, M.; Ohlanders, N.; Pellicciotti, F.; Williams, M.W.; McPhee, J. Estimating runoff from a glacierized catchment using natural tracers in the semi-arid Andes cordillera. *Hydrol. Processes* **2016**, *30*, 3609–3626. [CrossRef]
11. Tran, D.A.; Tsujimura, M.; Vo, L.P.; Nguyen, V.T.; Nguyen, L.D.; Dang, T.D. Stable isotope characteristics of water resources in the coastal area of the Vietnamese Mekong Delta. *Isot. Environ. Health Stud.* **2019**, *55*, 566–587. [CrossRef]
12. Qian, H.; Chen, J.; Howard, K.W.F. Assessing groundwater pollution and potential remediation processes in a multi-layer aquifer system. *Environ. Pollut.* **2020**, *263*, 114669. [CrossRef]
13. Giri, A.; Bharti, V.K.; Kalia, S.; Kumar, K.; Khansu, M. Hydrochemical and quality assessment of irrigation water at the trans-himalayan high-altitude regions of Leh, Ladakh, India. *Appl. Water Sci.* **2022**, *12*, 1–20. [CrossRef]

14. Zhao, X.F.; Chen, J.N.Y.; Tang, C.Y.; Zeng, S.Q.; Lu, Y.T. Hydrochemical characteristics and evolution of groundwater in a small catchment of Pearl River Delta. *Ecol. Environ. Sci.* **2007**, *16*, 1620–1626. [CrossRef]

15. Zhang, Y.; Cheng, R.; Zou, L.; Liang, Z.J.; Lv, W.; Dou, M.; Li, P.; Hu, Y.L.; Qi, X.B. The Effects of Climate Change and Anthropogenic Activities on Groundwater in Irrigation District. *J. Irrig. Drain.* **2022**, *41*, 91–100. [CrossRef]

16. Sun, H.Y.; Mao, Q.G.; Wei, X.F.; Zhang, H.Q.; Xi, Y.Z. Hydrogeochemical characteristics and formation evolutionary mechanism of the groundwater system in the Hami basin. *Geol. China* **2018**, *45*, 1128–1141.

17. Bodrud-Doza, M.; Islam, A.R.M.T.; Ahmed, F.; Das, S.; Saha, N.; Rahman, M.S. Characterization of groundwater quality using water evaluation indices, multivariate statistics and geostatistics in central Bangladesh. *Water Sci.* **2016**, *30*, 19–40. [CrossRef]

18. Fang, L.J.; Gao, R.Z.; Jia, D.B.; Yu, R.H.; Liu, X.Y.; Liu, T.X. Spatial-temporal characteristics of groundwater quality and its environmental driving factors of Steppe Basin—Taken Balaguer river basin of Inner Mongolia for instance. *China Environ. Sci.* **2021**, *41*, 2161–2169. [CrossRef]

19. He, Z.H.; Unger-Shayesteh, K.; Vorogushyn, S.; Weise, S.M.; Duethmann, D.; Kalashnikova, O.; Gafurov, A.; Merz, B. Comparing Bayesian and traditional end-member mixing approaches for hydrograph separation in a glacierized basin. *Hydrol. Earth Syst. Sci.* **2020**, *24*, 3289–3309. [CrossRef]

20. Liu, Z.; Qi, M.; Han, Y.; Cao, R.; Leng, J. Prediction of groundwater depression cone based on EMD-AR model in the irrigation area of the Lower Yellow River. *J. Henan Norm. Univ. (Nat. Sci. Ed.)* **2022**, *50*, 29–38. [CrossRef]

21. Ahmad, S.; Singh, N.; Mazhar, S.N. Hydrochemical characteristics of the groundwater in Trans-Yamuna Alluvial aquifer, Palwal District, Haryana, India. *Appl. Water Sci.* **2020**, *10*, 75. [CrossRef]

22. Cheng, C.H.; Deng, Y.X.; Zhuo, X.K.; Dai, D.; Yu, T. Changes in Water Chemistry and Driving Factors in the Middle and Lower Reaches of the Beijing-Hangzhou Grand Canal. *Environ. Sci.* **2021**, *42*, 2251–2259. [CrossRef]

23. Egbi, C.D.; Anornu, G.; Appiah-Adjei, E.K.; Ganyaglo, S.Y.; Dampare, S.B. Evaluation of water quality using hydrochemistry, stable isotopes, and water quality indices in the Lower Volta River Basin of Ghana. *Environ. Dev. Sustain.* **2019**, *21*, 3033–3063. [CrossRef]

24. Liu, F.; Zou, J.W.; Liu, J.R.; Zhang, J.K.; Zhen, P.N. Factors controlling groundwater chemical evolution with the impact of reduced exploitation. *CATENA* **2022**, *214*, 106261. [CrossRef]

25. Liu, J.T.; Gao, Z.J.; Wang, M.; Li, Y.Z.; Ma, Y.Y.; Shi, M.J.; Zhang, H.Y. Study on the dynamic characteristics of groundwater in the valley plain of Lhasa City. *Environ. Earth Sci.* **2018**, *77*, 646. [CrossRef]

26. Das, K.; Mukherjee, A. Depth-dependent groundwater response to coastal hydrodynamics in the tropical, Ganges river mega-delta front (the Sundarbans): Impact of hydraulic connectivity on drinking water vulnerability. *J. Hydrol.* **2019**, *575*, 499–512. [CrossRef]

27. Doveri, M.; Natali, S.; Franceschi, L.; Menichini, M.; Trifiro, S.; Giannecchini, R. Carbonate aquifers threatened by legacy mining: Hydrodynamics, hydrochemistry, and water isotopes integrated approach for spring water management. *J. Hydrol.* **2021**, *593*, 125850. [CrossRef]

28. Emvoutou, H.C.; Tandia, B.K.; Nkot, S.N.B.; Ebonji, R.C.S.; Nlend, Y.B.; Ekodeck, G.E.; Stumpp, C.; Maloszewski, P.; Faye, S. Geologic factors controlling groundwater chemistry in the coastal aquifer system of Douala/Cameroon: Implication for groundwater system functioning. *Environ. Earth Sci.* **2018**, *77*, 1–23. [CrossRef]

29. Huang, H.; Chen, Z.H.; Wang, T.; Zhang, L.; Zhou, G.M.; Sun, B.T.; Wang, Y. Characteristics and processes of hydrogeo-chemical evolution induced by long-term mining activities in karst aquifers, southwestern China. *Environ. Sci. Pollut. Res.* **2019**, *26*, 30055–30068. [CrossRef]

30. Liu, Z.; Zhao, Y.; Han, Y.; Wang, C.; Wang, F. Driving factors of the evolution of groundwater level in People's Victory Canal Irrigation District, China. *Desalination Water Treat.* **2018**, *112*, 325–333. [CrossRef]

31. *GB 11904-89*; Water Quality-Determination of Potassium and Sodium-Flame Atomic Absorption Spectrophotometry. MEE (Ministry of Ecology and Environment of the People's Republic of China): Beijing, China, 1990.

32. *GB 7477-87*; Water Quality-Determination of the Sum of Calcium and Magueslum—EDTA Titrimetrlc Method. MEE (Ministry of Ecology and Environment of the People's Republic of China): Beijing, China, 1987.

33. *HJ 84-2016*; Water Quality-Determination of Inorganic Anions($F-$, $Cl-$, $NO2-$, $Br-$, $NO3-$, $PO43-$, $SO32-$, $SO42-$)-Ion Chromatography. MEE (Ministry of Ecology and Environment of the People's Republic of China): Beijing, China, 2016.

34. *DZ/T 0064.49*; Methods for Analysis of Groundwater Quality Part 49: Determination of Carbonate, Bicarbonate Ions, Hydroxy. MNR (Ministry of Natural Resources of the People's Republic of China): Beijing, China, 1993.

35. Cui, J.Q.; Li, X.Y.; Shi, H.B.; Sun, Y.N.; An, H.J.; Xing, J.P. Chemical Evolution and Formation Mechanism of Groundwater in Hetao Irrigation Area. *Environ. Sci.* **2020**, *41*, 4011–4020. [CrossRef]

36. Cui, Y.H.; Wang, J.; Liu, Y.C.; HAO, S.; GAO, X. Hydro-chemical Characteristics and Ion Origin Analysis of Surface-groundwater in the Meeting Place of Shengjin Lake and Yangtze River. *Environ. Sci.* **2021**, *42*, 3223–3231. [CrossRef]

37. El Alfy, M.; Abdalla, F.; Moubark, K.; Alharbi, T. Hydrochemical equilibrium and statistical approaches as effective tools for identifying groundwater evolution and pollution sources in arid areas. *Geosci. J.* **2019**, *23*, 299–314. [CrossRef]

38. Huang, J.Z.; Xian, Y.; Li, W.; Zhang, D.Z.; Zhuang, X.M. Hydrogeochemical Evolution of Groundwater Flow System in the Typical Coastal Plain: A Case Study of Hangjiahu Plain. *Earth Sci.* **2021**, *46*, 2565–2582.

39. Keesari, T.; Pant, D.; Roy, A.; Sinha, U.K.; Jaryal, A.; Singh, M.; Jain, S.K. Fluoride Geochemistry and Exposure Risk Through Groundwater Sources in Northeastern Parts of Rajasthan, India. *Arch. Environ. Contam. Toxicol.* **2021**, *80*, 294–307. [CrossRef]

40. Marandi, A.; Shand, P. Groundwater chemistry and the Gibbs Diagram. *Appl. Geochem.* **2018**, *97*, 209–212. [CrossRef]

41. Mirza, A.; Rahman, M.T.; Saadat, M.; Islam, M.S.; Al-mansur, M.A.; Ahmed, S. Groundwater characterization and selection of suitable water type for irrigation in the western region of Bangladesh. *Appl. Water Sci.* **2017**, *7*, 233–243. [CrossRef]
42. Wali, S.; Umar, K.J.; Im, D.; Abubakar, S.D.; Ma, G.; Umar, A.; Aa, U. Groundwater Hydrochemical Characterization in Urban Areas of Southwestern Sokoto Basin, Nigeria. *Appl. Water Sci.* **2018**, *9*, 1006.
43. Wang, Y.J.; Song, X.F.; Li, B.H.; Ma, Y.; Zhang, Y.H.; Yang, L.H.; Bu, H.M.; Holm, P.E. Temporal variation in groundwater hydrochemistry driven by natural and anthropogenic processes at a reclaimed water irrigation region. *Hydrol. Res.* **2018**, *49*, 1652–1668. [CrossRef]
44. Wang, Y.S.; Li, S.; Li, H.X.; Cheng, X.X.; Li, W.P.; Zhang, M.N. Groundwater salinization characteristics and controlling factors in the Haiyuan Basin. *Hydrogeol. Eng. Geol.* **2019**, *46*, 10–17+57. [CrossRef]
45. Li, S.L.; Li, B.H.; Liu, H.J.; Qi, W.X.; Yang, Y.F.; Yu, G.; Qu, J.H. The biogeochemical responses of hyporheic groundwater to the long-run managed aquifer recharge: Linking microbial communities to hydrochemistry and micropollutants. *J. Hazard. Mater.* **2022**, *431*, 128587. [CrossRef] [PubMed]
46. Su, C.L.; Wang, Y.X.; Ge, S.M.; Li, Z.H.; Li, J.X. Origin of the Crescent Moon Spring in the Gobi Desert of northwestern China, based on understanding groundwater recharge. *J. Hydrol.* **2020**, *580*, 124344. [CrossRef]
47. Wang, J.L.; Jin, M.G.; Lu, G.P.; Zhang, D.; Kang, F.X.; Jia, B.J. Investigation of discharge-area groundwaters for recharge source characterization on different scales: The case of Jinan in northern China. *Hydrogeol. J.* **2016**, *24*, 1723–1737. [CrossRef]
48. Zhang, X.D.; Qian, H.; Wu, H.; Chen, J.; Qiao, L. Multivariate Analysis of Confined Groundwater Hydrochemistry of a Long-Exploited Sedimentary Basin in Northwest China. *J. Chem.* **2016**, *2016*, 3812125. [CrossRef]